DOI: 10.21062/mft.2023.082 http://www.journalmt.com

Machinability of UMCo50 Cobalt Superalloy

Oskar Zemčík (0000-0001-7786-3531), Karel Kouřil (0000-0003-0603-8053) Martin Slaný (0000-0002-9162-0066), Jan Zouhar (0000-0001-8031-8366), Josef Sedlák (0000-0002-9819-8259), Štěpán Kolomý (0000-0003-3781-692X) Institute of Manufacturing Technology, FME, Czech Brno University of Technology; Technická 2896/2, 61669 Brno, Czech Republic; zemcik.o@fme.vutbr.cz; Karel.Kouril@vutbr.cz; slany.m@fme.vutbr.cz; sedlak@fme.vutbr.cz; zouhar@fme.vutbr.cz; Stepan.Kolomy@vutbr.cz, Karel Kouřil was corresponding author

Testing of machinability of the UMCo50 superalloy was carried out within the project following the actual production of the semi-finished product by casting. Turning was chosen as the machining method to minimize the effect of an interrupted cut. Considering the machinability of a hard-to-machine alloy, the cutting material with the fine-grained WC-Co carbide with the TiN/TiAlN gradient PVD coating was selected. The progression of cutting forces, chip formation and tool wear were evaluated. Images of the material structure of the semi-finished product and the resulting chips were taken. From the measured values, graphs of the dependence of the chip thickness ratio on the cutting speed and the Taylor´s dependence of the tool durability on the cutting speed were obtained. The aim of the experiment was selection and verification of suitable cutting conditions for efficient machining of this superalloy, especially the appropriate value of the cutting speed. The recommended value of the cutting speed was 50-70 m.min^{-1}, while the tangential component of the cutting force was in the values usual for corrosion-resistant steels.

Keywords: UMCo50, Tool wear, Cobalt, Superalloy, Taylor's formula

1 Introduction

UMCo50 material belongs to the hard-to-machine cobalt-based superalloys [1-5] as is evident from its chemical composition. The main advantage of this alloy is its high wear and high temperature resistance. It also exhibits high creep resistance at higher temperatures and resistance to acids, mainly sulfuric and nitric acid. This alloy can also be found under the designation Cobalt 50, GCoCr28 or W.Nr 2.4778.

The tested cobalt alloy UMCo50 contains the stable hexagonal close-packed structure α-Co at a room temperature and it transforms into a face-centered cubic structure ε-Co at temperatures above 417 °C. During cooling from higher temperatures, a non-diffusion phase of martensitic transformation occurs. The contained chromium then leads to an increase in the transition temperature and stabilization of ε-Co [2,6,7].

When machining the UMCo50 material, significantly degraded machinability can be expected, requiring lower cutting speeds, high temperatures at the cutting point, and possible build-up edge and hardening of the material at the cutting point [1,8-14].

Superalloys are used, due to their properties, mainly in areas requiring extreme resistance both in terms of mechanical stress and extreme temperatures of the working environment [10,15-17]. Nickel and Cobalt based alloys are also used in the aerospace industry for thermally stressed parts [3,11,18]. An interesting application of cobalt alloys is in biomedicine [19,20]. Typical examples are protective layers in combustion heat exchangers [3,21,22]. The, the UmCO50 alloy itself is applied, for example, as a contact-stressed component in furnaces. This is due to its resistance to thermal shock and wear. The alloy also resists the influence of sulphur and vanadium impurities [17]. Another feature is its higher melting point compared to other cobalt base or nickel base heat-resistant alloys. The high melting point (1380~1395 °C) allows us to use it in furnaces, where other alloys usually cannot withstand, due to the fact that it has suitable mechanical properties even at extremely high temperatures [23].

In addition to the cast semi-finished products used in this experiment, the semi-finished products such as flat-rolled plates, forgings, welding wires, welded pipes and tubes, and seamless pipes and tubes are also available.

2 Materials and methods

The tested semi-finished product was produced by casting from a vacuum furnace into a block at the tapping temperature of 1600 °C and subsequently modified to a rotational shape by removing sprues on a band saw and turning to the diameter of 60 mm and the length of 400 mm. The chemical composition matched the required values, which can be seen in Table 1.

Tab. 1 *Chemical composition of UMCo-50 [20]*

Co[%]	Cr[%]	Fe[%]	Ni[%]	Mo[%]	Mn[%]	Si[%]	C[%]	S,P[%]
48-52	27-29	21	2-2.5	1-1.5	0.5-1	0.5-1	0.05-0.12	<0.02

Turning was chosen as a machining method. The parameters tested included cutting edge wear, cutting forces and the resulting surface finish and chip formation. The chemical composition of the sample, its microstructure and hardness were also checked and corresponded to the assumption of [20]. The cutting material with a fine-grained carbide substrate (< 1 μm) with a PVD made TiN/TiAlN gradient coating, mainly due to the expected better resistance to built-up edge (BUE) [11]. The reference material (grade 14b) was also machined for comparison. The TOS SU 50 A 1500 lathe with additional automatic speed control was used. The Zwick Roell ZHR hardness tester allows to measure the hardness according to Rockwell. The hardness was measured using the HRA method at the load of 60 kgf with the Brale indenter. The Kistler type 9257B apparatus was used to measure the cutting forces and for verification of the chemical composition the X-MET 8000 X-ray analyser was used. Wear measurements on the flank were performed using the Zeiss Stemi 2000-C microscope with the Axiocam 105 color camera attached. The TR 100 Surface 100 Roughness Tester was used to measure the surface roughness Ra.

The value of cutting speed was tested from 40 m.min^{-1} to 110 m.min^{-1}. No active cooling was used. The cutting tool ISO DCLNR 2525 M12 with the insert CNMG 120404E-NF T8330 was used. All cutting inserts were visually inspected before use. The feed rate was f = 0.2 mm.rev^{-1} and the depth of cut was ap = 1 mm. The main controlled parameter was the flank wear VB with the limit value of 0.25 mm and it was used to find the basic Taylor's formula coefficients.

$$v_c = \frac{c_{\varpi\tau}}{\frac{1}{T^m}} [m \cdot \mu\iota\nu^{-1}] \quad (1)$$

Where:
cvt…Constant [-],
m…Taylor exponent [-].
T…Durability [min].
vc…Cutting speed [m.min^{-1}].

As additional values, the resulting shape, chips deformation, their structure and the course of cutting forces were also evaluated. The roughness of the machined surface was checked, which was intended to provide a better overview of the investigated process [8]. The resulting chip thickness was measured with the Mitutoyo digital caliper. For each cutting speed tested, a minimum of 20 measurements were taken and the mean value calculated.

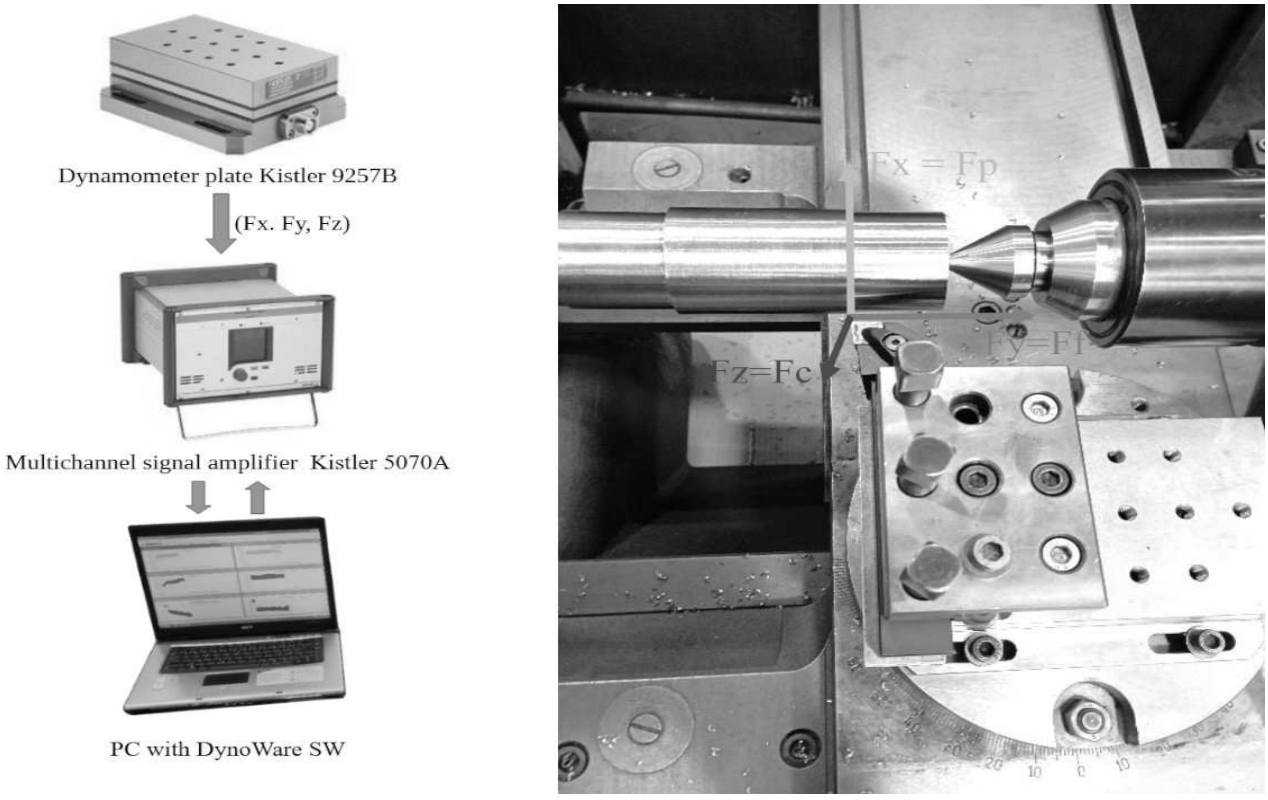

Fig. 1 *Measurement scheme using a Kistler dynamometer*

3 Results and discussion

Figure 2 shows the structure of the machined semi-finished product at 200x, respectively 1000x magnification. The surface was etched using the Marble mixture (~25 ml HCl, ~25 ml ethanol, ~5g CuSO4). This was the structure of the cast semi-finished product [9], which was subsequently modified to a rotational shape by removing sprues and turning to a diameter of 60 mm and a length of 400 mm.

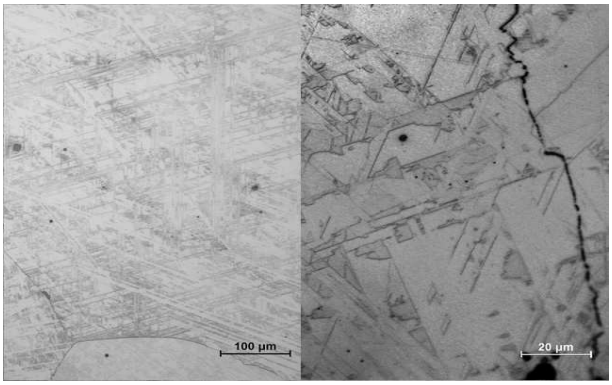

Fig. 2 *Microstructure of tested UMCo-50, cast semi-finished product*

The resulting hardness of the machined sample reached 58 – 61 HRA, which corresponds to 220 – 250 HV, in contrast to the expected hardness of 320 HV according to [3].

Precise evaluation of the flank wear with the help of a digital workshop microscope was carried out at regular time intervals (10 s for higher than 90 m.min^{-1}, 20 s for lower cutting speeds), so that it was possible to complete the given time interval per cut on several different cutting edges. Then, in the resulting graph the mean values were used. The end of life of the cutting insert is usually caused by chipping of the cutting edge or tip or by melting due to high temperature in the cutting zone [24]. Based on this, a VB wear threshold was also determined, beyond which critical damage to the insert would occur, making a stable cut impossible. Any instability or intermittent cutting also greatly contributes to the initiation of brittle failure of the cutting insert [24, 25]. The monitored surface roughness reached Ra = 2.4 µm for a feed rate of 0.2 mm.rev^{-1}, Ra = 0.8 µm for a feed rate of 0.1 mm.rev^{-1} and Ra = 4.8 µm for f = 0.3 mm.rev^{-1}. There were no significant deviations with the change in cutting speed. From the dependence of tool wear on the time in cut, the resulting durability times were then subtracted for the selected critical wear value of 0.25 mm. Their logarithmic value was used to construct the resulting Taylor´s graph.

Figure 3 clearly shows the wear pattern of the cutting inserts for the speeds 50 and 90 m.min^{-1}, which were typical in the tested range of cutting speeds. At the 90 m.min^{-1}, the part of the build-up due to the composition of the machined material and the cutting insert is most noticeable.

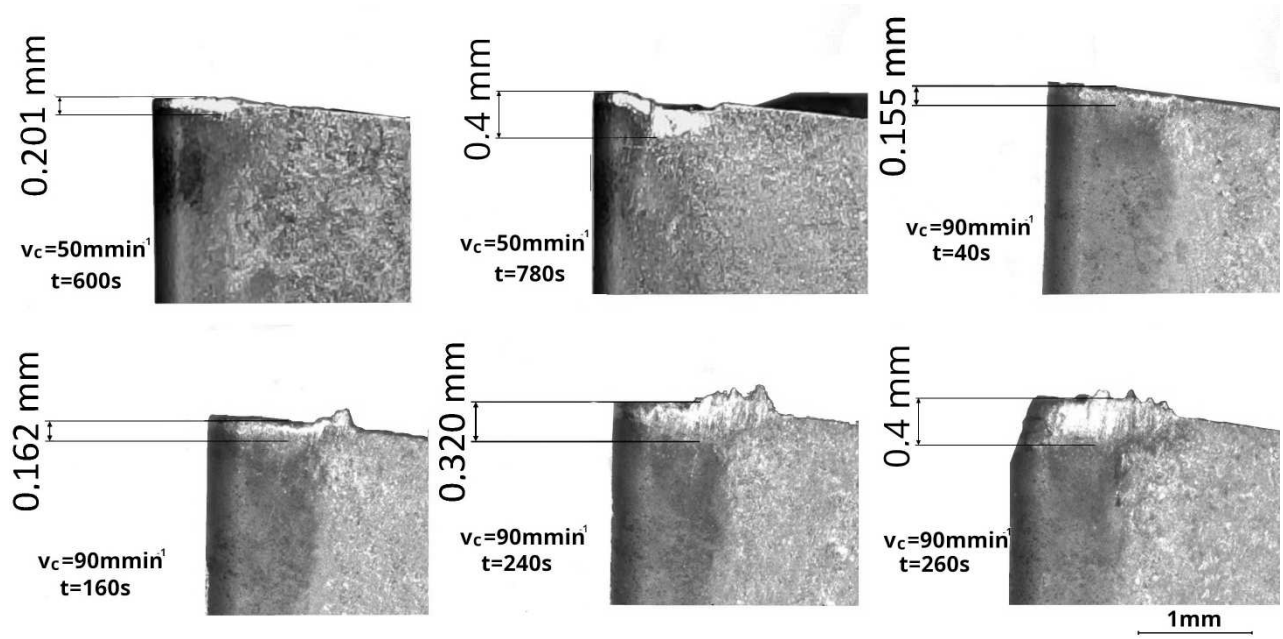

Fig. 3 *Flank wear VB for 50 and 90 m.min^{-1}*

The value of the cutting speed significantly influences the amount of energy delivered to the cutting point. It is largely converted into thermal energy and then, it has a negative effect on both the workpiece material and the tool.

At speeds above 80 m.min^{-1}, overheating occurred in the cutting-edge area, which had a significant effect on tool durability in turn. Therefore, the application of cooling is appropriate to ensure greater durability.

The flank wear progression is shown for different

cutting speeds in Figure 3. As expected, the wear progression is divided into three phases. At first, there is a sharp increase in VB, it is followed by a relatively stable phase and then, it is concluded by a renewed sharp increase in wear and eventual destruction of the cutting insert edge. The graph clearly shows the increase in the value of cutting insert durability with decreasing cutting speed value. Therefore, the steepest dependence corresponds to 110 m.min^{-1} and the least steep to 40 m.min^{-1}. The deviations in the progress are given due to the number of inserts tested and, in particular, for the curve representing 40 m.min^{-1}, to premature damage to one of the inserts. This could have been caused by both a defect in the particular cutting insert or a possible error in the testing material. The values represent the mean value of three different cutting edges.

Tab. 2 *Measured wear values of VB depending on time t*

t[min]	VB [mm]							
	vc [m.min^{-1}]							
	40	50	60	70	70	90	100	110
0.30	0.05	0.06	0.05	0.06	0.05	0.05	0.05	0.05
0.50	0.10	0.11	0.08	0.12	0.08	0.10	0.13	0.10
1.00	0.12	0.12	0.14	0.15	0.10	0.11	0.17	0.20
1.50	0.15	0.13	0.14	0.16	0.11	0.13	0.25	0.30
2.00	0.16	0.14	0.14	0.17	0.12	0.15	0.35	-
2.50	0.16	0.14	0.15	0.18	0.14	0.26	-	-
3.00	0.16	0.15	0.15	0.19	0.17	0.35	-	-
3.50	0.16	0.15	0.15	0.20	0.30	-	-	-
4.00	0.16	0.16	0.16	0.20	-	-	-	-
4.50	0.16	0.16	0.16	0.21	-	-	-	-
5.00	0.17	0.16	0.16	0.22	-	-	-	-
5.50	0.17	0.16	0.16	0.23	-	-	-	-
6.00	0.17	0.17	0.17	0.24	-	-	-	-
6.50	0.17	0.17	0.17	0.25	-	-	-	-
7.00	0.18	0.17	0.17	0.27	-	-	-	-
7.50	0.18	0.17	0.17	0.30	-	-	-	-
8.00	0.18	0.17	0.18	-	-	-	-	-
8.50	0.18	0.18	0.18	-	-	-	-	-
9.00	0.19	0.18	0.18	-	-	-	-	-
9.50	0.19	0.19	0.20	-	-	-	-	-
10.00	0.19	0.20	0.25	-	-	-	-	-
10.50	0.20	0.21	0.35	-	-	-	-	-
11.00	0.20	0.23	-	-	-	-	-	-
11.50	0.21	0.25	-	-	-	-	-	-
12.00	0.21	0.28	-	-	-	-	-	-
12.50	0.22	0.30	-	-	-	-	-	-
13.00	0.22	-	-	-	-	-	-	-
16.00	0.23	-	-	-	-	-	-	-
20.00	0.24	-	-	-	-	-	-	-
27.00	0.30	-	-	-	-	-	-	-

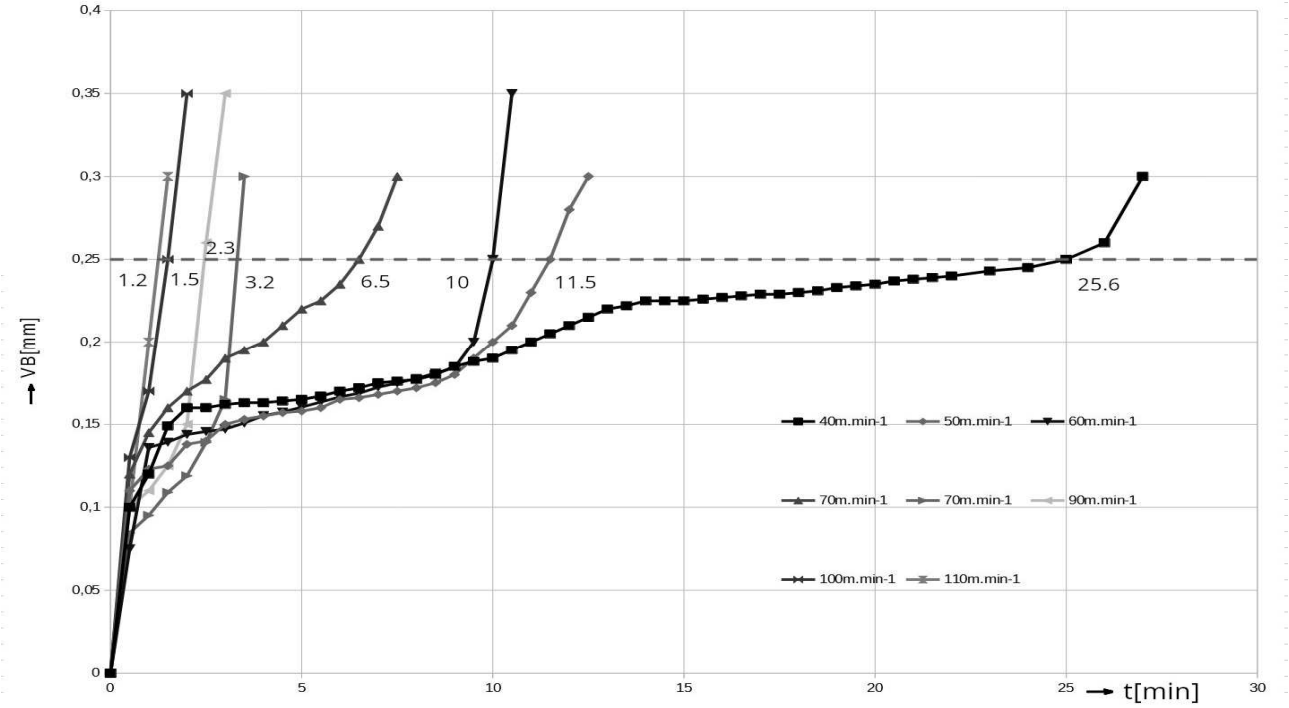

Graph 1 *Dependence of tool flank wear VB on time*

The read values from Graph 1 were entered into Graph 2 of the Taylor´s dependence after logarithmization (see Table 2 and 3). Then, the plotted values were fitted with a straight line using the least squares method, i.e. linear regression. The equation of such a straight line of the form y = ax+b or in this case y = -ax+b actually represents the Taylor´s dependence itself, where "y" corresponds to the logarithm of the durability, "a" to the exponent "m", "x" to the logarithm of the cutting speed and "b" to the CT constant from the equation 1.

The value of the coefficient of determination R2 = 0.977 indicates a high rate of result agreement.

Tab. 3 *Durability readings for different cutting speeds*

vc[m.min^{-1}]	40	50	60	70	80	90	100	110
T[min]	25.6	11.5	10	6.5	3.2	2.3	1.46	1.2
Log (vc)	1.602	1.699	1.778	1.845	1.903	1.954	2	2.041
Log (T)	1.408	1.060	1	0.813	0.505	0.362	0.164	0.079

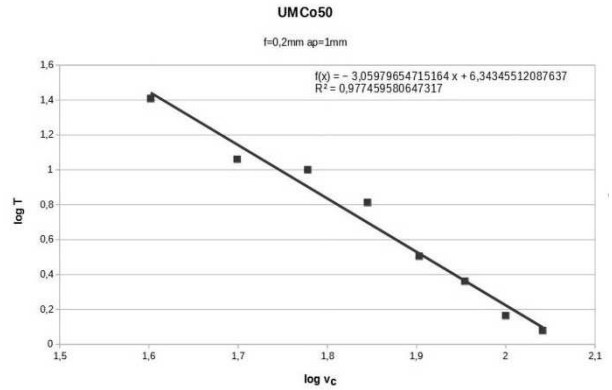

Graph 2 *The resulting Taylor's formula*

In order to ensure the adequate tool life and the quality of the machined surface, it is also advisable to measure the cutting force components [8]. Three basic components were measured, i.e. a tangential Fc, passive Fp and feed Ff. Their assignment and orientation can be seen in Figure 1.

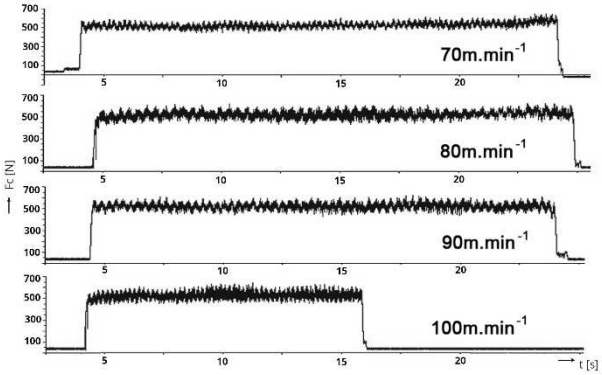

Fig. 4 *Cutting force for different cutting speeds Fc [N]*

The cutting force value ranged from 450 N to 600 N, with the value of over 700 N for the worn tool, which corresponded to the specific cutting force of 2750 MPa, without feed correction. Using feed correction and the Kienzle model. The resulting value is kc11 = 1800 MPa for the Kienzle exponent mc = 0.26 [26].

Figure 4 shows the progress of the tangential component Fc of the cutting force, which corresponded to the value of the direction Fz in the experiment, for 4 different cutting speeds. The higher density of variation of the measured value corresponds to higher revolutions of the workpiece for higher cutting speeds and at the same time a decreasing diameter of the machined sample.

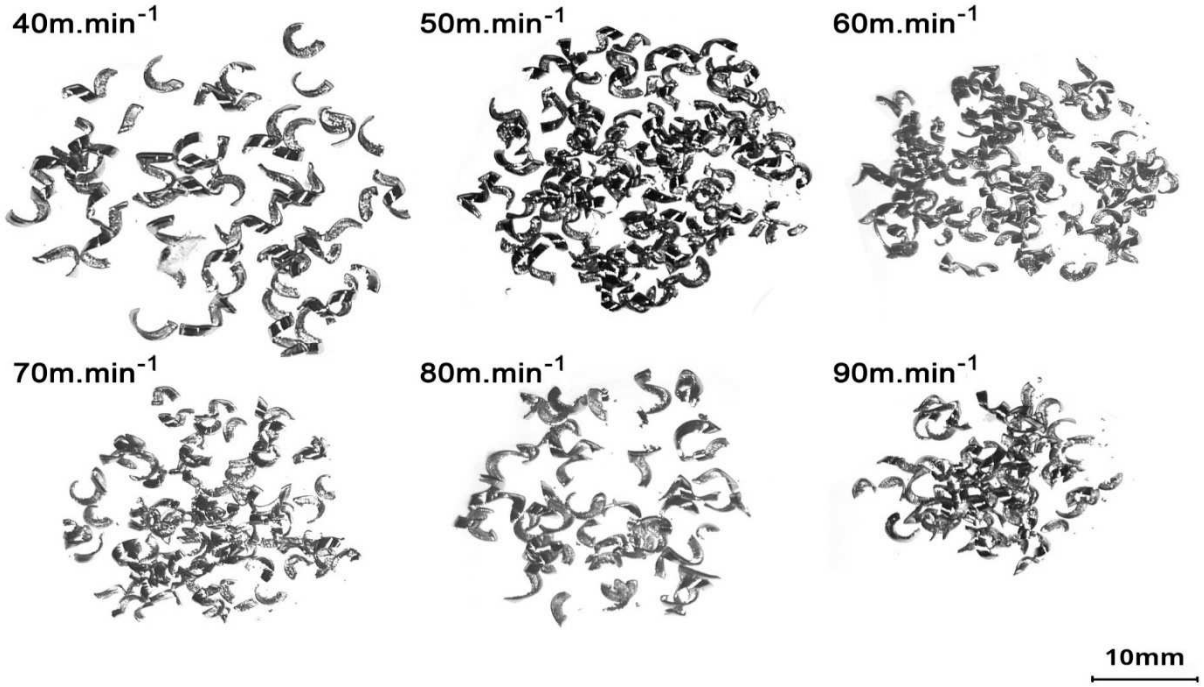

Fig. 5 *Chip shape for cutting speeds of 40 – 90 m.min1*

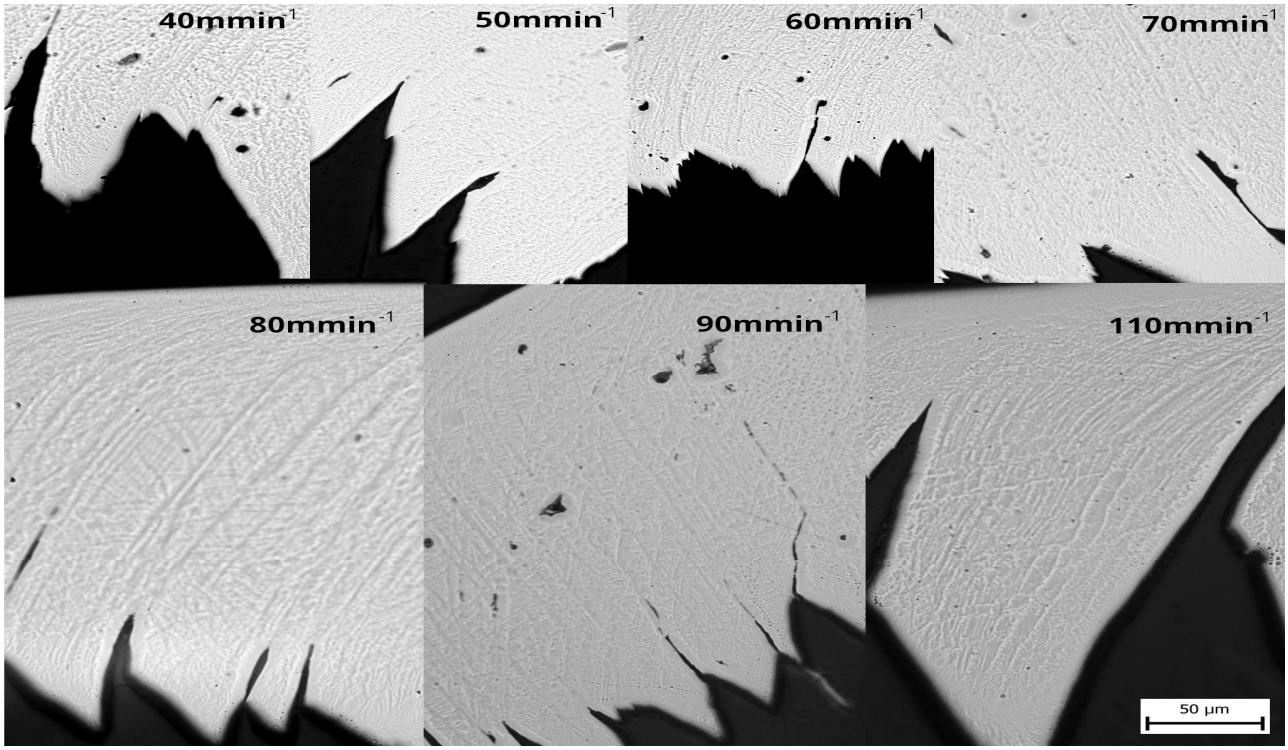

Fig. 6 *Chip structure for cutting speeds of 40–110 m.min1*

In terms of a stable cut, a continuous chip is usually considered ideal. However, this is inappropriate in the context of automated machining and the need to ensure that the chip can easily move away from the cutting point. Therefore, the cutting conditions are preferably set so that the chip is divided into smaller segments [27]. Both the working geometry of the tool and other cutting conditions, especially the cutting speed, influence the chip shape [28-31].

The angle of the shear plane and thus the chip reduction coefficient is influenced, besides the working geometry of the tool, by the coefficient of friction in the chip material and therefore by the properties of the material to be machined under the given conditions [33]. As the cutting speed increases, the temperature at the cutting point also increases, especially in the shear plane, and affects both the tool durability and the contoured shape of the chip [34].

In Figure 6, the areas in which plastic deformation of the chip material and the formation of individual cells occurred are visible for all cutting speeds. The width of the individual shear segments varied between 10 and 100 μm. In the area of the chip in contact with the tool face, a homogeneous structure is evident.

The shape of the chip, from long coma chips to spiral chips, was consistent throughout the range of tested cutting speeds (see Fig. 5). The chip reduction coefficient, defined as the ratio of the thickness of the resulting chip to the uncut chip thickness given by the feed and the angle of the main blade, reached its lowest value at 80 m.min^{-1} approximately Ks = 1.32.

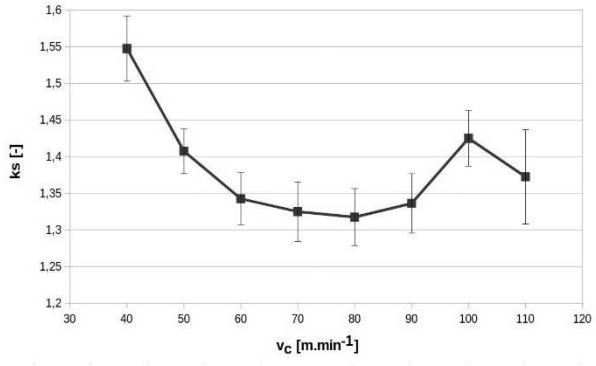

Graph 3 *Chip reduction coefficient on cutting speed*

At higher values of cutting speeds there were also larger deviations of the measured values, which can be seen at the end of Graph 3, especially at 110 m.min^{-1}.

4 Conclusions

The verified parameters apply to ranges corresponding to feeds around f = 0.2 mm.rev^{-1} and ap = 1 mm.

A suitable cutting speed value corresponds to 50 m.min^{-1} and can be increased up to 70 m.min^{-1} using suitable cooling of the cutting point.

The material has a significantly worse machinability compared to the standard steels, corresponding to the machinability coefficient Kv = 0.167, which would correspond to the machinability class 6b, when compared to a steel standard.

The Taylor's formula coefficients are m = 3.06, CT = 6.343 and Cv = 2.073. It is advisable to provide suitable cooling during machining and to select a resistant coating to prevent build-up edge. At cutting speeds above 80 m.min^{-1}, the durability of the blade was already highly unstable, which was also manifested by larger variations in the cutting force values.

The value of the specific cutting force corresponded to Kc = 2750MPa. Without correction of the effect of feed on the specific cutting force [26]. When choosing the cutting material, it is also necessary to take the high cobalt content of the alloy into account, which can lead to growth on the sintered carbide cutting inserts, especially after coating damage.

Acknowledgement

This research was supported by the project No. TK04020189 within the public tender in the THETA program of the Czech Ministry of Industry and Trade.

References

[1] ZAMAN, HAINOL AKBAR, SAFIAN SHARIF, DONG-WON KIM, MOHD HASBULLAH IDRIS, MOHD AZLAN SUHAIMI A Z. TUMURKHUYAG. Machinability of Cobalt-based and Cobalt Chromium Molybdenum Alloys - A Review. *Procedia Manufacturing [online]*. 2017, 11, 563-570 [cit. 2023-04-09]. ISSN 23519789. From: doi:10.1016/j.promfg.2017.07.150

[2] XUE, HAITAO, DONG ZHOU, WEIBING GUO, XIAOPING LUAN, TAO LI A JIANGLONG ZHAO. Cobalt-based alloy surfacing process optimization and surfacing material performance analysis. *Materials Research Express [online]*. 2021, 8(2) [cit. 2023-04-09]. ISSN 2053-1591. From: doi:10.1088/2053-1591/abdf1b

[3] XUE, HAITAO, XIAOPING LUAN, WEIBING GUO A DONG ZHOU. Microstructure and properties of TIF surfacing Co-based alloy on UMCo50 process burner. *Archives of Metallurgy and Materials*. 2022, 67(1), 14-30. From: doi:10.24425/amm.2022.137467

[4] THELLAPUTTA, GOPALA RAO, PULCHARU SUBHASH CHANDRA A C.S.P. RAO. Machinability of Nickel Based

Superalloys: A Review. *Materials Today: Proceedings*. 2017, 4(2), 3712-3721. ISSN 22147853. From:10.1016/j.matpr.2017.02.266

[5] DE BROUWER, J.L., A. DAVIN a D. COUTSOURADIS. Some applications of cobalt containing heat resistant alloys. Metallurgy and Uses, *Proceedings. Brussels: Benelux Metall*, 1981, digitized 2 Oct 2009, 1981(VOl. 2), 187-195.

[6] LÓPEZ, H.F. a A.J. SALDIVAR-GARCIA. Martensitic Transformation in a Cast Co-Cr-Mo-C Alloy. METALLURGICAL AND MATERIALS TRANSACTIONS A. 2008, 39(1), 8-18. ISSN 1073-5623. From: 10.1007/s11661-007-9370-8

[7] VACCHIERI, E., A. COSTA, G. RONCALLO a G. CACCIAMANI. Service induced fcc→hcp martensitic transformation in a Co-based superalloy. *Materials Science and Technology*. 2017, issue 18(volume 33), 1100-1107. ISSN 0267-0836. From: doi:doi.org/10.1080/02670836.2016.1273866

[8] SHAH, SAURABH, ANAND JOSHI, KAMLESH CHAUHAN, ANKIT OZA, CHANDER PRAKASH, RAUL DUARTE SALGUEIRAL GOMES CAMPILHO A SANDEEP KUMAR. Feasibility Analysis of Machining Cobalt-Chromium Alloy (Stellite-6) Using TiN Coated Binary Inserts. *Materials*. 2022, 15(20), 1-14. ISSN 1996-1944. From: doi:10.3390/ma15207294

[9] MARY JASMIN, N., Y. ANIL REDDY, A. ANU KUTTAN, APPANA NIKHIL, J. VENKATA SURESH, S. SAMPATH REDDY A RAM SUBBIAH. Experimental investigation of Machining of stellite alloy. *Materials Today: Proceedings*. 2022, 66, 665-669. ISSN 22147853. From: doi:10.1016/j.matpr.2022.03.635

[10] HOESEL, DANNY, et al. "Milling of cast material and PTA-hard-facing layers of the cobalt-base-alloy stellite 12." *Annals of DAAAM & Proceedings*, annual 2011, pp. 949+. Gale Academic OneFile, link.gale.com/apps/doc/A349222888/AONE?u=googlescholar&sid=bookmark-AONE&xid=df30daa6. Accessed 14 July 2023.

[11] EZUGWU, E. O., Z. M. WANG a C. I. OKEKE. Tool Life and Surface Integrity When Machining Inconel 718 With PVD- and CVD-Coated Tools. *Tribology Transactions*. 1999, 42(2), 353-360. ISSN 1040-2004. From: doi:10.1080/10402009908982228

[12] MA LJ, YU H, MAO XH, LI CR, FENG CY, LI FN. Influence of Cutting Tool and Drilling Process on the Machinability of Inconel 718. *Manufacturing Technology*. 2023;23(2):204-215. doi: 10.21062/mft.2023.013.

[13] PETRU J, SCHIFFNER J, ZLAMAL T, SADILEK M, STANCEKOVA D. Investigations of Cutting Tool Wear While Machining Inconel 718. *Manufacturing Technology*. 2015;15(3):396-403. doi: 10.21062/ujep/x.2015/a/1213-2489/MT/15/3/396.

[14] DAŇA M, ZETEK M, SCHORNÍK V. Cutting Tool Life when Tapping Nickel Based Super Alloy. *Manufacturing Technology*. 2017;17(1):18-23. doi: 10.21062/ujep/x.2017/a/1213-2489/MT/17/1/18.

[15] DAVIS, J.R., ed. ASM Specialty Handbook: Nickel, Cobalt, and Their Alloys. *OH, USA: ASM International: Novelty*, 2000. ISBN 978-0-87170-685-0.

[16] ABEL, Lois A., ed. ASM handbook: nonferrous alloys and special-purpose materials Volume 2 Properties and selection. *10th ed. Materials Park*, USA: ASM International, 1990. ISBN 08-717-0378-5.

[17] OUAMPAN, SIRIWAN, SIAM KAEWKUMSAI A EKKARUT VIYANIT. Sulfidation failure of UMCo-50 protective sheath tube used for a temperature monitoring device exposed to sulfur dioxide bearing hot gas. *Engineering Failure Analysis*. 2022, 2022(vol. 138), Article 106218. ISSN 1350-6307. From: doi:10.1016/j.engfailanal.2022.106218

[18] ZEBALA, WOJCIECH, GRZEGORZ STRUZIKIEWICZ A KSENIA RUMIAN. Cutting Forces and Tool Wear Investigation during Turning of Sintered Nickel-Cobalt Alloy with CBN Tools. *Materials*. 2021, 7(14), 1-22. ISSN 1996-1944. From: doi:doi.org/10.3390/ma14071623

[19] ANDERSEN, P.J. 1.1 Metals for Use in Medicine. *Comprehensive Biomaterials II*. Elsevier, 2017, 2017, 1-18. ISBN 9780081006924. From: doi:10.1016/B978-0-08-100691-7.00247-0

[20] URBAIN, M., BLAVIER, P. & COUTSOURADIS, D. Structure, properties, and applications of UMCo-50 alloy. *JOM* 16, 837–842 (1964). https://doi.org/10.1007/BF03378301

[21] SLANÝ, MARTIN, JOSEF SEDLÁK, OSKAR ZEMČÍK, JAN ZOUHAR et al.

Material and Dimensional Analysis of Bimetallic Pipe Bend with Defined Bending Radii. *Tehnicki vjesnik - Technical Gazette*. 2021, 28(3), 974-982. ISSN 13303651. From: doi:10.17559/TV-20200409093723

[22] SLANY, MARTIN, JOSEF SEDLAK, JAN ZOUHAR, OSKAR ZEMČÍK, et al. Analysis of bimetal pipe bends with a bend of 0.7D with a cladding layer of Inconel 625. *The International Journal of Advanced Manufacturing Technology*. 2021, 117(11-12), 3859-3871. ISSN 0268-3768. From: doi:10.1007/s00170-021-07749-1

[23] SATO, J., T. OMORI, K. OIKAWA, I. OHNUMA, R. KAINUMA a K. ISHIDA. Cobalt-Base High-Temperature Alloys. *Science*. 2006, 312(5770), 90-91. ISSN 0036-8075. From: doi:10.1126/science.1121738

[24] ALTAN, ERHAN, ALPER UYSAL, ŞEREF HAN ANAÇ A SABRI ÖZTÜRK. Effect of work hardening of cobalt in sintered carbide cutting tool on tool failure during interrupted cutting. *The International Journal of Advanced Manufacturing Technology*. 2017, 88(1-4), 359-367. ISSN 0268-3768. From: doi:10.1007/s00170-016-8765-3

[25] AYKUT, ŞEREF, EYUP BAGCI, AYKUT KENTLI A OSMAN YAZICIOĞLU. Experimental observation of tool wear, cutting forces and chip morphology in face milling of cobalt based super-alloy with physical vapour deposition coated and uncoated tool. *Materials and Design*. 2007, 28(6), 1880-1888. ISSN 02613069. From: doi:10.1016/j.matdes.2006.04.014

[26] VELCHEV, STEPHAN, IVAN KOLEV A KRASIMIR IVANOV. Empirical mathematical models of the dependence of the specific cutting force on thickness of cut in turning. *Annals of faculty engineering hunedoara: International Journal of Engineering*. Romania: University Politehnica Timisoar, 2011, roč. 9, č. 5, s. 303-312. ISSN 584 – 2673.

[27] ÖPÖZ, TAHSIN TECELLI A XUN CHEN. Chip Formation Mechanism Using Finite Element Simulation. *Strojniški vestnik - Journal of Mechanical Engineering*. 2016, 62(11), 636-646. ISSN 00392480. From: doi:10.5545/sv-jme.2016.3523

[28] BARON, SZYMON A EAMONN AHEARNE. Fundamental mechanisms of chip formation in orthogonal cutting of medical grade cobalt chromium alloy (ASTM F75). *CIRP Journal of Manufacturing Science and Technology*. 2018, 11(23), 54-63. ISSN 17555817. From: doi:10.1016/j.cirpj.2018.09.002

[29] DE ALMEIDA, S. M., M. MIERNIK a H. ZEBROWSKI. Influence of microstructure on chip formation and machinability of some cobalt alloys. *Materials Science and Technology*. 2013, 4(4), 366-370. ISSN 0267-0836. From: doi:10.1179/mst.1988.4.4.366

[30] HUA, YANG A ZHANQIANG LIU. Experimental Investigation of Principal Residual Stress and Fatigue Performance for Turned Nickel-Based Superalloy Inconel 718. *Materials*. 2018, 11(6), 1-15. ISSN 1996-1944. From: doi:10.3390/ma11060879

[31] XIE, J.Q., A.E. BAYOUMI a H.M. ZBIB. A study on shear banding in chip formation of orthogonal machining. *International Journal of Machine Tools and Manufacture*. 1996, 36(7), 835-847. ISSN 08906955. From: doi:10.1016/0890-6955(95)00016-X

[32] SIMA, MOHAMMAD A TUĞRUL ÖZEL. Modified material constitutive models for serrated chip formation simulations and experimental validation in machining of titanium alloy Ti–6Al–4V. *International Journal of Machine Tools and Manufacture*. 2010, 50(11), 943-960. ISSN 08906955. From: doi:10.1016/j.ijmachtools.2010.08.004

[33] BIL, HALIL, S.ENGIN KILIÇ A A.ERMAN TEKKAYA. A comparison of orthogonal cutting data from experiments with three different finite element models. *International Journal of Machine Tools and Manufacture*. 2004, 44(9), 933-944. ISSN 08906955. From: doi:10.1016/j.ijmachtools.2004.01.016

[34] CALAMAZ, M., D. COUPARD, M. NOUARI a F. GIROT. Numerical analysis of chip formation and shear localisation processes in machining the Ti-6Al-4V titanium alloy. *The International Journal of Advanced Manufacturing Technology*. 2011, 52(9-12), 887-895. ISSN 0268-3768. From: doi:10.1007/s00170-010-2789-x